# Geometric Effect of Au Nanoclusters on Room Temperature CO Oxidation

| Journal: | *ChemComm* |
|---|---|
| Manuscript ID | CC-COM-10-2019-008381.R1 |
| Article Type: | Communication |
| | |

SCHOLARONE™
Manuscripts

# COMMUNICATION

## Geometric Effect of Au Nanoclusters on Room Temperature CO Oxidation†

Yafeng Cai,[a,b] Yun Guo[b] * and Jingyue Liu[a] *

**We report the effect of *in situ* transforming ZnO supported single Au atoms to 3-dimensional Au clusters ($Au_{3D}$) on room temperature CO oxidation activity. We discovered that an intermediate, highly distorted 2-dimensional $Au_{layer}$ species are much more active than both the $Au_{3D}$ clusters and the Au single atoms. The geometric arrangement of Au clusters and their interactions with support surfaces play a pivotal role in determining their catalytic performance for room temperature CO oxidation on ZnO supported Au catalysts.**

The prominent size effect of metal nanoparticles (NPs), due to the change of coordination number, chemical state and metal support interaction with particle size, have been widely proposed to account for the experimentally observed catalytic performance of supported metal catalysts for various important chemical transformations[1-6]. The most striking example is that supported smaller Au NPs possess substantial catalytic activity for many reactions (e.g., CO oxidation) while larger Au NPs are essentially inactive[7-9]. Although the origin of highly active nano Au for CO oxidation has been intensively investigated it still remains a controversial topic on the nature of the most active forms of Au species. To date, size of Au species[10, 11], bilayer Au nanostructures[10, 11], Au charge states[12, 13], and Au-metal oxide interfacial perimeters[14-16] were all proposed to account for the unique catalytic properties of nanostructured Au species. Most experimental studies focused on Au NPs with sizes ranging from 2 to 5 nm. The study of the catalytic properties of ultra-small (< 2 nm) Au species on various supports should be of both scientific interest and practical importance. Theoretical studies show that ultra-small Au clusters may have significant geometric effects[17, 18]. Mavrikakis et al[19] found that expansion strain in Au clusters can increase the reactivity of Au and such strain effect increases rapidly with decreasing cluster size. In practice, most supported metal catalysts often contain metal single atoms, nanoclusters and various sizes of NPs, and such heterogeneity

of potential active species hampers deeper understanding of how each individual species contributes to the observed activity[20]. Supported Au single-atom catalysts (SACs) have been synthesized by wet-chemistry method[5, 20, 21]. However, facile synthesis of supported Au clusters with narrow size distributions and better defined morphology is still a challenge.

Very recently, several research groups[13, 22, 23] used supported metal atoms as precursor to obtain supported Au cluster catalysts by reduction and/or calcination treatment. Such an approach helps distinguish the contributions of different Au species (single atoms, nanoclusters and NPs) to the total CO oxidation activity. It should be mentioned, however, that both the reduction and/or calcination treatment of supported metal SACs not only change the nature of the metal species but also modifies the nature of the support as well as the metal-support interactions[24]. In this work, we report an *in situ* transformation of Au single atoms to 3D nanoclusters ($Au_{3D}$) through an intermediate Au monolayer configuration ($Au_{layer}$) during room temperature CO oxidation. Our experimental results unambiguously demonstrate that the $Au_{layer}$ configuration yielded the highest reactivity. Both the Au single atoms and the $Au_{3D}$ clusters do not possess the highest activity. This work also demonstrates that even at ambient temperature Au single atoms sinter rapidly on ZnO surfaces under CO environment and that the most active $Au_{layer}$ clusters are not stable either. Strong support-induced distortion of the $Au_{layer}$ nanoclusters is proposed to be responsible for the observed high activity for room temperature CO oxidation.

Flower-like 2D ZnO nanosheets with average thickness of 9 nm was prepared by a hydrothermal method and the subsequent calcination to eliminate organic species (Fig. S1-S3). The $Au_1$/ZnO SAC with 0.78 wt.% of Au (determined by ICP-AES) was prepared by room temperature UV-assisted photochemical deposition of Au single atoms onto the as-synthesized 2D ZnO flower-like powders. The details on the sample synthesis, characterization and reaction evaluation are provided in the ESI†. The specific area of the $Au_1$/ZnO SAC was measured to be 46.6 $m^2 \cdot g^{-1}$, according to the Brunauer-Emmett-Teller (BET) method, by $N_2$ adsorption isotherm (Fig. S4). X-ray diffraction pattern of the $Au_1$/ZnO catalyst showed only the characteristic peaks of wurtzite ZnO (Fig. S5). Representative atomic resolution HAADF-STEM image (Fig. 1a) shows exclusively Au single atoms (marked by red circles) uniformly dispersed on the surfaces of the ZnO support. Careful examination of different sample regions

[a.] Department of Physics, Arizona State University, Tempe, Arizona 85287, United States. E-mail: Jingyue.liu@asu.edu
[b.] Key Laboratory for Advanced Materials and Research Institute of Industrial Catalysis, School of Chemistry and Molecular Engineering, East China University of Science and Technology, 130 Meilong Road, Shanghai 200237, China. E-mail: yunguo@ecust.edu.cn

COMMUNICATION

revealed that only Au single atoms were present in the Au$_1$/ZnO SAC and these Au atoms occupy the exact positions of the Zn cations on the ZnO surfaces (Fig. S6).
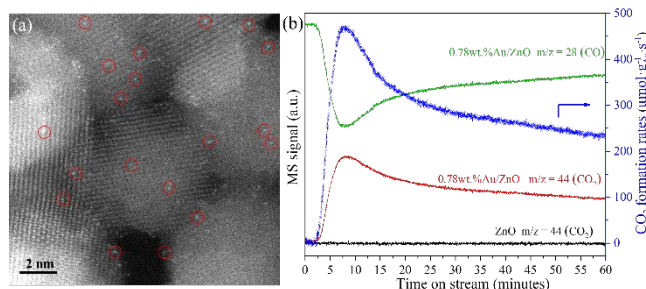


**Fig. 1** (a) Representative HAADF-STEM image of Au$_1$/ZnO SAC. Au single atoms are marked by red circles. For clarity, only a few isolated Au atoms are circled although many more are present in the image. (b) Time-dependent CO$_2$ (m/z = 44) signals during CO oxidation over the 0.78 wt.% Au$_1$/ZnO SAC (red plot) and the ZnO support (black plot). The CO$_2$ formation rate with reaction time (blue plot) is displayed in unit of μmol/(g$_{Au}$·s).

We tested CO oxidation over the Au$_1$/ZnO SAC by measuring the CO$_2$ signal (m/z = 44) with an on-line mass spectrometer (Fig. 1b). It should be noted that no CO$_2$ molecules were released during the first 2 minutes of CO introduction, indicating that the Au$_1$/ZnO SAC was either not active or needed a longer incubation time. However, the CO$_2$ signal then increased rapidly with reaction time: the CO$_2$ formation rate increased quickly to a maximum (461.5 μmol·$g_{Au}^{-1}$·s$^{-1}$) at ~8 minutes. If we assume that all the Au atoms were accessible we obtain a turnover frequency of 9.14×10$^{-2}$ s$^{-1}$. When the CO oxidation proceeds further, the CO$_2$ formation rate decreased gradually to 205.1 μmol·$g_{Au}^{-1}$·s$^{-1}$ after ~60 minutes. Such a time-dependent reaction rate suggests that the catalyst structure continuously evolved. There was no observable CO$_2$ formation on the pristine ZnO support, suggesting that the observed CO$_2$ molecules exclusively originated from the Au species.

For low temperature CO oxidation, the accumulation of surface carbonate species is usually considered to be one of the main reasons for deactivation[25, 26]. To verify if the carbonate species played a major role on our catalyst, temperature programed desorption of CO$_2$ under He flow environment was conducted immediately after 60 minutes of CO oxidation (Fig. S7). There were little CO$_2$ desorbed from the used catalyst suggesting that the activity decrease was not caused by strong adsorption of CO$_2$ or accumulation of carbonate species.

Detailed electron microscopy study was conducted on the Au/ZnO catalysts after CO oxidation for 4, 8 and 60 minutes. A gas-flow reaction setup was used to treat the samples (Scheme S2). As discussed above, the fresh catalyst contained only Au single atoms. However, after room temperature CO oxidation for 4 minutes, Au nanoclusters with an average size of 0.9 nm were formed (Fig. 2) and simultaneously the number density of the single Au atoms significantly decreased (Fig. S8). Therefore, ZnO supported single Au atoms started sintering as soon as the room temperature CO oxidation started. When CO oxidation proceeds further, statistical analyses of more than 300 Au clusters from each sample indicated that the average size of the Au clusters did not change appreciably (Fig. 2d) with an average size of 0.9 nm after 8 min and a slightly larger average size of 1.1 nm after 60 min. Some single Au atoms were still present in these samples although the number density of the single Au atoms decreased by ~97.7% after 60 min of CO oxidation (Fig.

S8). The number density of Au clusters changed appreciably for 8 min CO oxidation from that of 60 min, suggesting that the total number of Au atoms in each Au cluster changed significantly although their sizes did not change much.

The activity of Au catalysts for CO oxidation is, in general, predominantly affected by the size of the Au species and the redox property of the support[27]. In this work, the ZnO support does not possess high redox capability, especially at ambient temperatures. Our experimental data, however, clearly shows that the Au clusters with similar sizes yielded very different activity. These results suggest that the geometric configuration of Au clusters may have an important role in CO oxidation.
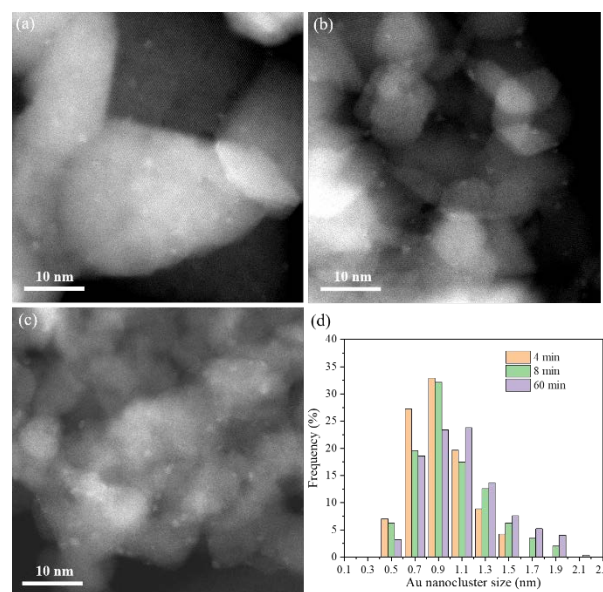


**Fig. 2** Representative HAADF-STEM images of Au/ZnO after CO oxidation for (a) 4 minutes, (b) 8 minutes, and (c) 60 minutes. The size distributions of the Au nanoclusters after different times of CO oxidation reaction (d) did not show significant changes.

To understand the relationship between the Au geometric configuration and catalytic performance, we analyzed the atomic arrangement of Au atoms in the Au nanoclusters. After 4 min, monolayers of Au species (Au$_{layer}$) were observable (Fig. 3a) with ~0.25 and ~0.28 nm lattice spacings, similar to the spacings of ZnO(101) and ZnO(100), in contrast to bulk Au lattice spacings of d$_{Au(111)}$ = 0.24 nm and d$_{Au(200)}$ = 0.20 nm. After 8 min, in addition to Au$_{layer}$, Au$_{3D}$ clusters appeared (indicated by the yellow squares in Fig. 3b-c). The measured lattice spacings of these Au$_{layer}$ (~0.25 and ~0.26 nm) still match well with ZnO(101) and ZnO(002), but much larger than those of bulk Au. After 60 min, the Au$_{layer}$ species were not detectable and only Au$_{3D}$ nanoclusters and a tiny amount of single Au atoms were detected, suggesting that the transformation of Au single atoms to Au$_{3D}$ nanoclusters completed. The few Au atoms that still persisted on the ZnO surfaces could have occupied the Zn cation vacancy positions. The monolayer Au$_{layer}$ species seem to be the transient intermediate state of transforming single Au atoms to Au$_{3D}$ nanoclusters during the CO oxidation reaction. The Au$_{3D}$ nanoclusters (Fig. 3f) showed lattice spacings of 0.20 and 0.24 nm, matching well with that of bulk Au{200} and Au{111} spacings.

The atomic resolution HAADF studies clearly show that 1) the majority of the as-prepared Au single atoms are not stable under CO environment, 2) the stabilized Au clusters take 3D

shape with lattice spacings close to bulk Au, and 3) the transient 2D monolayer species are significantly distorted in order to form an epitaxial relationship with the ZnO support. Austin and co-workers[17] conducted DFT calculations of the shape effect on the adsorption behavior of small Au nanoclusters (~1 nm) and found that planar Au nanoclusters would transit to Au3D at high CO coverage. Our experimental results seem to support this conclusion for ZnO supported Au species.
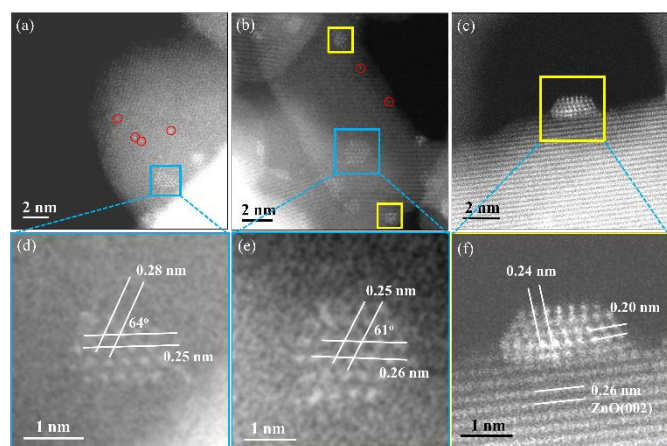


**Fig. 3** Representative atomic-resolution HAADF-STEM images of Au/ZnO catalyst after CO oxidation for (a, d) 4 minutes, (b, e) 8 minutes, and (c, f) 60 minutes. Au single atoms, $Au_{layer}$ and $Au_{3D}$ nanoclusters are marked by red circles, cyan squares and yellow squares, respectively. The magnified images (d-f) correspond to the cyan squares in (a, b) and the yellow square in (c), respectively.

Based on the experimental results, we can deduce the following structural change of the Au atoms during room temperature CO oxidation: Under CO environment, single Au atoms assemble to initially form highly distorted $Au_{layer}$ that aligns with the support lattice spacings and then the $Au_{layer}$ species transform to $Au_{3D}$ when the $Au_{layer}$/ZnO interfacial energy becomes larger. If we assume that the CO conversion rate on the ZnO supported single Au atoms is small or negligible and that the highly distorted 2D $Au_{layer}$ species are most active then we can fully understand the time dependent behavior of the $CO_2$ formation rate. The reactivity of these ZnO supported Au species follows the sequence $Au_{layer} > Au_{3D} >> Au_1$.

To gain detailed information about the chemical states of the different Au species, fresh $Au_1$/ZnO SAC and after 4, 8 and 60 minutes of CO oxidation were immediately examined by XPS (Fig. S9, Fig. 4a). Although most of the Au 4f peaks were buried under the strong Zn $3p_{3/2}$ peak (Fig. S10), a small shoulder peak is clearly observable at ~85 eV in the fresh $Au_1$/ZnO. This peak can be assigned to positively charged Au species $(Au^{\delta+})$[28-31]. Phala and co-workers[32] found, by DFT calculations, that oxidized Au can be stabilized at $Zn^{2+}$ positions in the bulk terminated surface sites. Our STEM imaging results also showed that Au single atoms are located on the positions of $Zn^{2+}$ sites (not necessarily the $Zn^{2+}$ vacancies) (Fig. 1a and S6). The interaction between the Au atoms and the ZnO surface oxygen induces electron transfer from the Au atoms to the ZnO support, yielding the high content of $Au^{\delta+}$. When CO oxidation started the content of the $Au^{\delta+}$ species drastically decreased while the amount of the $Au^0$ species increased (Fig. 4b). The XPS data clearly show that the change of Au oxidation state followed the structural change of the Au species. *In situ* DRIFTS study of the as-prepared $Au_1$/ZnO under CO oxidation conditions (Fig. S11) shows that the relative $CO_2$/CO adsorption peak ratio increased

dramatically during the first several minutes of reaction, reached the maximum at ~8 min, and then slowly decreased, corroborating the activity results of Fig. 1b.
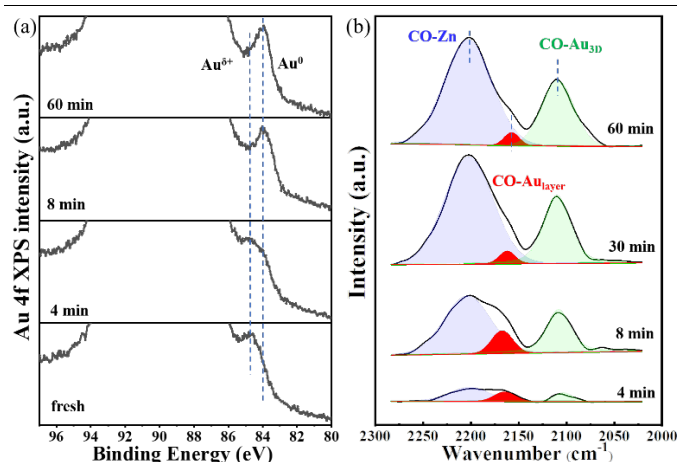


**Fig. 4** (a) High resolution XPS spectra of Au 4f core-level of Au/ZnO for CO oxidation after different time intervals (0, 4, 8 and 60 minutes). (b) IR spectra of CO adsorbed on Au/ZnO at room temperature after reaction for different time intervals (4, 8, 30 and 60 minutes). The band of CO adsorbed on $Au_{layer}$ species at different time intervals is highlighted in red in each XPS spectrum.

To further understand the nature of the active Au species we conducted CO-DRIFTS experiments on the $Au_1$/ZnO SAC. After each specified reaction time, the residual gas was purged with pure Ar and then the CO-DRFITS spectra were taken (Fig. 4b). Three adsorption bands were identified at around 2200, 2110, and 2165 $cm^{-1}$, respectively. The band at ~2110 $cm^{-1}$ can be assigned to CO adsorption on $Au^0$ sites[33, 34]. The band at ~2200 $cm^{-1}$ can be assigned to CO adsorption on $Au^{3+}$ sites[35, 36] or CO adsorption on ZnO[37-39]. The CO adsorption band on $Au^{3+}$ sites is considered to be extremely weak and is difficult to be even detected since $Au^{3+}$ is normally coordinately saturated and can be easily reduced to $Au^{\delta+}$ by CO[23, 35, 40]. Both the XPS and the STEM imaging data suggest that with reaction time the $Au^0$ species should increase and the high valence Au species should decrease. Since Fig. 4b shows that the intensity of the 2200 $cm^{-1}$ band increases with reaction time the assignment of this band to $Au^{3+}$ is not plausible. It was reported that CO could adsorb on ZnO at 2200 $cm^{-1}$ in the presence of $CO_2$ [37-39]. We detected CO adsorption on treated ZnO at about 2190 $cm^{-1}$ under similar conditions (Fig. S12). Therefore, we assigned the 2200 $cm^{-1}$ band to CO adsorption on Zn cations. As discussed above, the isolated Au atoms move to form $Au_{layer}$ and $Au_{3D}$ as reaction proceeds. The CO molecules that adsorb on the active Au clusters react with surface oxygen species on the ZnO to produce $CO_2$ and simultaneously create more exposed $Zn^{2+}$ sites around the Au species. Both the migration of Au atoms and the oxidation of the adsorbed CO molecules lead to the increased intensity of CO adsorption on exposed Zn cation sites.

The shoulder band centered at ~2165 $cm^{-1}$ can be assigned to CO adsorption on $Au^{\delta+}$ sites[41]. After deconvolution of the adsorption bands, one can observe that the peak area of the 2165 $cm^{-1}$ $Au^{\delta+}$ band first increased, reached a maximum at ~8 min, and then decreased gradually. This time dependent change of the amount of $Au^{\delta+}$ sites coincides with the time dependent change of the CO oxidation activity (Fig. 1b) and the formation of the $Au_{layer}$ (Fig. 3). The STEM images showed that the $Au_{layer}$ species possess a longer Au-Au bond which should possess a

stronger adsorption strength of CO than that on $Au_{3D}$ due to strain induced effects[18],[19]. The strong interaction between the $Au_{layer}$ and the ZnO surface facilitates electron transfer from the Au species to the ZnO support, resulting in larger amount of positively charged Au species. When the $Au_{3D}$ were formed the perimeter Au atoms may behave similarly to the $Au_{layer}$ species and CO adsorption at $Au^{\delta+}$ sites still existed but with a smaller amount. The excellent match between the amounts of the $Au^{\delta+}$ sites with the CO oxidation activity further confirms that the $Au_{layer}$ species with $Au^{\delta+}$ sites exhibit the highest activity.

In summary, our work shows highly distorted monolayer Au species as most active sties for room temperature CO oxidation on ZnO supported Au catalysts. Both ZnO supported Au atoms and $Au_{layer}$ species, however, are not stable: They evolve into 3D Au clusters. ZnO supported single Au atoms are not active for room temperature CO oxidation. For small Au clusters, cluster geometry and their electronic interaction with support surfaces are critical. This work provided deeper insights into the structure-performance relationship of supported Au species.

## Conflicts of interest

There are no conflicts to declare.

## Notes and references

1. B. Roldan Cuenya and F. Behafarid, *Surf. Sci. Rep.*, 2015, **70**, 135-187.
2. K. An and G. A. Somorjai, *Catal. Lett.*, 2015, **145**, 233-248.
3. S. Cao, F. Tao, Y. Tang, Y. Li and J. Yu, *Chem. Soc. Rev.*, 2016, **45**, 4747-4765.
4. B. R. Cuenya, *Thin Solid Films*, 2010, **518**, 3127-3150.
5. L. Liu and A. Corma, *Chem. Rev.*, 2018, **118**, 4981-5079.
6. T. Takei, T. Akita, I. Nakamura, T. Fujitani, M. Okumura, K. Okazaki, J. H. Huang, T. Ishida and M. Haruta, *Advances in Catalysis, Vol 55*, 2012, **55**, 1-126.
7. M. Haruta, T. Kobayashi, H. Sano and N. Yamada, *Chem. Lett.*, 1987, **16**, 405-408.
8. M. Haruta, *Catal. Today*, 1997, **36**, 153-166.
9. G. J. Hutchings, *ACS Central Science*, 2018, **4**, 1095-1101.
10. M. Valden, X. Lai and D. W. Goodman, *Science*, 1998, **281**, 1647-1650.
11. A. A. Herzing, C. J. Kiely, A. F. Carley, P. Landon and G. J. Hutchings, *Science*, 2008, **321**, 1331-1335.
12. A. Y. Klyushin, M. T. Greiner, X. Huang, T. Lunkenbein, X. Li, O. Timpe, M. Friedrich, M. Hävecker, A. Knop-Gericke and R. Schlögl, *ACS Catal.*, 2016, 3372-3380.
13. S. Wei, X.-P. Fu, W.-W. Wang, Z. Jin, Q.-S. Song and C.-J. Jia, *J. Phys. Chem. C*, 2018, **122**, 4928-4936.
14. M. Haruta, *Faraday Discuss.*, 2011, **152**, 11-32.
15. Y. Y. Wu, N. A. Mashayekhi and H. H. Kung, *Catal. Sci. Technol.*, 2013, **3**, 2881.
16. B. Shao, J. Zhang, J. Huang, B. Qiao, Y. Su, S. Miao, Y. Zhou, D. Li, W. Huang and W. Shen, *Small Methods*, 2018, **0**, 1800273.
17. N. Austin, J. K. Johnson and G. Mpourmpakis, *J. Phys. Chem. C*, 2015, **119**, 18196-18202.
18. J.-X. Liu, I. A. W. Filot, Y. Su, B. Zijlstra and E. J. M. Hensen, *J. Phys. Chem. C*, 2018, **122**, 8327-8340.
19. M. Mavrikakis, P. Stoltze and J. K. Nørskov, *Catal. Lett.*, 2000, **64**, 101-106.
20. J. Liu, *ACS Catal.*, 2017, **7**, 34-59.
21. Z. Li, D. Wang, Y. Wu and Y. Li, *Natl. Sci. Rev.*, 2018, **5**, 673-689.
22. J. Wang, H. Y. Tan, S. Z. Yu and K. B. Zhou, *ACS Catal.*, 2015, **5**, 2873-2881.
23. L.-W. Guo, P.-P. Du, X.-P. Fu, C. Ma, J. Zeng, R. Si, Y.-Y. Huang, C.-J. Jia, Y.-W. Zhang and C.-H. Yan, *Nat. Commun.*, 2016, **7**, 13481.
24. T. Fujita, T. Ishida, K. Shibamoto, T. Honma, H. Ohashi, T. Murayama and M. Haruta, *ACS Catal.*, 2019, **9**, 8364-8372.
25. P. Konova, A. Naydenov, C. Venkov, D. Mehandjiev, D. Andreeva and T. Tabakova, *J. Mol. Catal. A: Chem.*, 2004, **213**, 235-240.
26. Y. Hao, M. Mihaylov, E. Ivanova, K. Hadjiivanov, H. Knözinger and B. C. Gates, *J. Catal.*, 2009, **261**, 137-149.
27. X. Y. Liu, A. Wang, T. Zhang and C.-Y. Mou, *Nano Today*, 2013, **8**, 403-416.
28. D. Boyd, S. Golunski, G. R. Hearne, T. Magadzu, K. Mallick, M. C. Raphulu, A. Venugopal and M. S. Scurrell, *Appl. Catal., A*, 2005, **292**, 76-81.
29. M. P. Casaletto, A. Longo, A. Martorana, A. Prestianni and A. M. Venezia, *Surf. Interface Anal.*, 2006, **38**, 215-218.
30. K. Qian, W. Huang, J. Fang, S. Lv, B. He, Z. Jiang and S. Wei, *J. Catal.*, 2008, **255**, 269-278.
31. M. Han, X. Wang, Y. Shen, C. Tang, G. Li and R. L. Smith, *J. Phys. Chem. C*, 2009, **114**, 793-798.
32. N. S. Phala, G. Klatt, E. van Steen, S. A. French, A. A. Sokol and C. R. A. Catlow, *Phys. Chem. Chem. Phys.*, 2005, **7**, 2440-2445.
33. M. Manzoli, A. Chiorino and F. Boccuzzi, *Appl. Catal., B*, 2004, **52**, 259-266.
34. F. Boccuzzi, A. Chiorino, S. Tsubota and M. Haruta, *Catal. Lett.*, 1994, **29**, 225-234.
35. M. Mihaylov, H. Knözinger, K. Hadjiivanov and B. C. Gates, *Chem. Ing. Tech.*, 2007, **79**, 795-806.
36. M. Mihaylov, B. C. Gates, J. C. Fierro-Gonzalez, K. Hadjiivanov and H. Knözinger, *J. Phys. Chem. C*, 2007, **111**, 2548-2556.
37. Y. Wang, X. Xia, A. Urban, H. Qiu, J. Strunk, B. Meyer, M. Muhler and C. Wöll, *Angew. Chem. Int. Ed.*, 2007, **46**, 7315-7318.
38. H. Noei, C. Wöll, M. Muhler and Y. Wang, *Appl. Catal., A*, 2011, **391**, 31-35.
39. H. Noei, A. Birkner, K. Merz, M. Muhler and Y. Wang, *J. Phys. Chem. C*, 2012, **116**, 11181-11188.
40. X. P. Fu, L. W. Guo, W. W. Wang, C. Ma, C. J. Jia, K. Wu, R. Si, L. D. Sun and C. H. Yan, *J. Am. Chem. Soc.*, 2019, **141**, 4613-4623.
41. M. Mihaylov, E. Ivanova, Y. Hao, K. Hadjiivanov, H. Knözinger and B. C. Gates, *J. Phys. Chem. C*, 2008, **112**, 18973-18983.
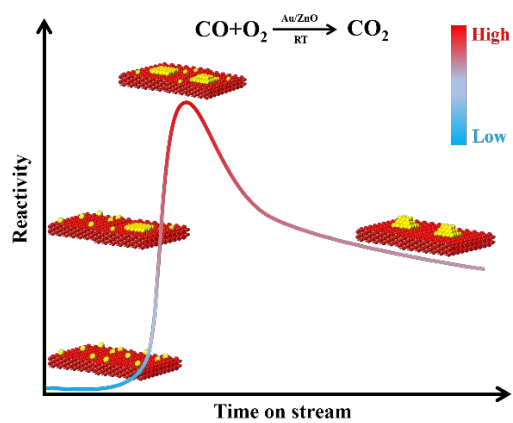
ZnO supported highly distorted Au monolayers are most active for room temperature CO oxidation.